Influence of Viscosity Coefficient Variation in Discrete Adjoint Method

Deng Jun[1], Zhao Ke[1], Zhang Wei[1], Huang Jiangtao[2], Xia Lu[1] and Gao Zhenghong[1]

[1]School of Aeronautics, Northwestern Polytechnical University, Xi'an, China
zhaokecfd@163.com
[2]Aerospace Technology, Institute of China Aerodynamic Research and Development Center, Mianyang, China

Abstract. The economy of aircraft has received more and more attention, and the influence of the constant viscosity assumption in discrete adjoint system on the optimization would no longer be ignored. In this paper, we studied the influence of constant viscosity assumption on the stability of the adjoint equation and gradient accuracy. In the viscosity coefficient variation, the laminar viscosity was treated by the Sutherland criterion and the turbulence viscosity was studied by the SA and SST turbulence model, respectively. The ONERA M6 case was adopted to make comparisons of the convergence history of the adjoint equation and the gradient accuracy. The convergence history showed that the viscosity coefficient variation did not significantly affect the stability of the adjoint equation. The gradient variation due to the viscosity coefficient variation at the shock wave separation region was very distinct from the shock-free region, indicating that the viscosity variation could not be ignored in the design problems with large viscous effects, such as shock wave boundary layer interference separation. To furtherly research the influence of the constant viscosity assumption on the aerodynamic optimization design, the optimization benchmark CRM was carried out firstly with the constant viscosity assumption, then restarted with the viscosity variation in second stage. It was presented that the optimization results in second stage could furtherly improve the aerodynamic performance of the aircraft, demonstrating that the variation of the viscosity coefficient also had a significant effect on the shock-free region. From the assessment above, the viscosity variation could significantly improve the accuracy in gradient computation, maintaining the computational stability and convergence. Therefore, the assumption of constant viscosity was not suitable for the high-fidelity aircraft design.

Keywords: Discrete Adjoint Method, Aerodynamic Optimization, Viscosity Variation, Gradient Accuracy.

1 Introduction

Intense market competition and severe operational requirements required continuous improvement of the comprehensive performance of aircraft. Therefore, improving the performance of aircraft had always been the focus of aircraft design. Researchers

had made efforts to reduce each count of drag, and formed optimization design methods, such as surrogate model based optimization and gradient based optimization methods. In order to further improve the performance of aircraft, researchers had carried research on refined design methods for aircraft. The refined design of aircraft was a high-dimensional design problem. The optimization design system based on gradient had high efficiency in dealing with large-scale design variable problems, and the calculation amount of gradient based on adjoint method was almost independent of the number of design variables. The gradient of the objective function on the design variable could be quickly obtained by one control equation solving and one adjoint equation solving. Therefore, it had attracted much attention from researchers and had been widely applied in the fields such as aerodynamic[1, 2], structural[3, 4], sonic boom[5], electromagnetic[6, 7].

In the aspect of aerodynamic design, researchers in various countries had deeply studied the aerodynamic gradient calculation method based on adjoint method, and formed a large number of aerodynamic adjoint optimization design systems. NASA had developed a discrete adjoint optimization system[8] based on the unstructured grid solver FUN3D; DLR had developed the discrete adjoint optimization systems based on the structured grid solver Flower and the unstructured grid solver TAU[9]; ONERA had developed a discrete adjoint optimization system[10] based on elsA; The team of Professor Martins from the University of Michigan developed the AD Flow discrete adjoint design system[11]. Zuo Yingtao, et al.[12] of Northwestern Polytechnical University established a discrete adjoint optimization design system based on N-S equation; Li Bin, et al.[13] of China Aerodynamics Research and Development Center established the discrete adjoint system optimization design system based on unstructured grid solver; Huang Jiangtao et al.[2] established a discrete adjoint optimization system of structured grid based on the large-scale parallel CFD code PMB3D developed by CARDC.

The accuracy and robustness of aerodynamic adjoint method mainly depended on the inviscid term. Currently, the discrete adjoint systems mainly used the central scheme[2, 9, 10] on the inviscid term. However, there was a problem of insufficient robustness in a wide range of velocity domains. There also used upwind scheme on the inviscid term of adjoint equation[14], which had strong robustness in complex states. In the aerodynamic adjoint method, the viscous term was also an important part. When high-precision inviscid term was used in the adjoint equation, the treatment of the viscous term determined the gradient accuracy. In the treatment of viscous term, due to the variational treatment of viscosity coefficient was complex, the main discrete adjoint design systems[2, 9, 10] mostly adopted the constant viscosity assumption. or used the automatic differentiation[15] to derive simple turbulence model, with low calculation efficiency. In the context of refined aircraft design, in order to further improve the aerodynamic performance of the aircraft, the influence of the constant viscosity assumption on the gradient could not be ignored.

Focused on the influence of flow viscosity on the adjoint field and gradient, based on the Sutherland criterion, Spalart Allmaras, and Menter's k-ω SST turbulence model, this article conducted research on viscosity coefficient variation, derived the aerodynamic adjoint equation of viscosity coefficient variation in discrete form, and cou-

pled the viscosity coefficient adjoint to the adjoint optimization design system developed by the research group. On the optimization results of the cruise state of the CRM wing body which using the assumption of constant viscosity, the optimization design of viscosity coefficient variation was carried out, and the drag was further reduced, verifying the effectiveness of the method.

2 Viscosity Coefficient Variation

The typical flow field adjoint equation was as follows:

$$\frac{\partial I}{\partial \mathbf{Q}} + \boldsymbol{\lambda}^T \frac{\partial \boldsymbol{R}}{\partial \mathbf{Q}} = 0 \tag{1}$$

where I was the design objective function, $\boldsymbol{Q}$ was the flow field conservation variable, and $\boldsymbol{R}$ was the residual of the flow field obtained by solving the N-S Equation. The point of the adjoint method was to perform variational treatment on the residual term of the flow field to obtain the left term of the adjoint equation:

$$\boldsymbol{\lambda}^T \frac{\partial \boldsymbol{R}}{\partial \mathbf{Q}} = \boldsymbol{\lambda}^T \frac{\partial \boldsymbol{R}_c}{\partial \mathbf{Q}} - \boldsymbol{\lambda}^T \frac{\partial \boldsymbol{R}_v}{\partial \mathbf{Q}} \tag{2}$$

where $\boldsymbol{R}_c$ was the residual of the inviscid term in the flow field and $\boldsymbol{R}_v$ was the residual of the viscous term. This article adopted the inviscid term[14] of the adjoint equation derived by the Van Leer scheme; In the viscous term, we usually used the assumption of constant viscosity to simplify the complexity of the program, ignoring the influence of viscosity coefficient variation on the adjoint field. For viscous flow, the assumption of constant viscosity was sufficient to obtain good design results. In order to further improve the performance of the optimization design system and the aerodynamic performance of the aircraft, this paper considered the influence of viscosity coefficient on the adjoint field and gradient.

2.1 Viscous Term of Adjoint Equation Under the Assumption of Constant Viscosity Coefficient

In curvilinear coordinates (ξ, η, ζ), the derivation in three directions had the same consistent form. When using the assumption of constant viscosity coefficient, the variation of viscosity term in the ξ direction was:

$$\delta \boldsymbol{R}_{v,i} = \delta \boldsymbol{F}_{v,i+1/2} - \delta \boldsymbol{F}_{v,i-1/2} \tag{3}$$

where:

$$\begin{aligned} \delta \boldsymbol{F}_{v,i+1/2}(\boldsymbol{q}) &= \delta \boldsymbol{F}_{v,l,i+1/2}\left(\boldsymbol{q}\left(\boldsymbol{Q}_i, \boldsymbol{Q}_{i+1}\right)\right) \\ &= \frac{\partial \boldsymbol{F}_{v,l,i+1/2}}{\partial \boldsymbol{q}_i} \frac{\partial \boldsymbol{q}_i}{\partial \boldsymbol{Q}_i} \delta \boldsymbol{Q}_i + \frac{\partial \boldsymbol{F}_{v,l,i+1/2}}{\partial \boldsymbol{q}_{i+1}} \frac{\partial \boldsymbol{q}_{i+1}}{\partial \boldsymbol{Q}_{i+1}} \delta \boldsymbol{Q}_{i+1} \end{aligned} \tag{4}$$

Therefore, the Eq. (4) could be written as:

$$\begin{aligned}\delta \boldsymbol{R}_{v,i} = &\frac{\partial \boldsymbol{F}_{v,l,i+1/2}}{\partial \boldsymbol{q}_i}\frac{\partial \boldsymbol{q}_i}{\partial \boldsymbol{Q}_i}\delta \boldsymbol{Q}_i + \frac{\partial \boldsymbol{F}_{v,l,i+1/2}}{\partial \boldsymbol{q}_{i+1}}\frac{\partial \boldsymbol{q}_{i+1}}{\partial \boldsymbol{Q}_{i+1}}\delta \boldsymbol{Q}_{i+1} - \\ &\frac{\partial \boldsymbol{F}_{v,l,i-1/2}}{\partial \boldsymbol{q}_{i-1}}\frac{\partial \boldsymbol{q}_{i-1}}{\partial \boldsymbol{Q}_{i-1}}\delta \boldsymbol{Q}_{i-1} + \frac{\partial \boldsymbol{F}_{v,l,i-1/2}}{\partial \boldsymbol{q}_i}\frac{\partial \boldsymbol{q}_i}{\partial \boldsymbol{Q}_i}\delta \boldsymbol{Q}_i\end{aligned} \tag{5}$$

In the above equation, there were three stencils that contribute to this cell, so there were seven stencils under three-dimensional condition. Multiplying the above equation by the adjoint variable λ and summing to obtain:

$$\begin{aligned}\sum \boldsymbol{\lambda}_{i,j,k}^T \delta \boldsymbol{R}_v(i,j,k) = &+...+\boldsymbol{\lambda}_{i-1,j,k}^T \delta \boldsymbol{R}_v(i,j,k)+ \\ &\boldsymbol{\lambda}_{i,j,k}^T \delta \boldsymbol{R}_v(i,j,k)+\boldsymbol{\lambda}_{i+1,j,k}^T \delta \boldsymbol{R}_v(i,j,k)+...\end{aligned} \tag{6}$$

Merging the items that contain $\delta \boldsymbol{Q}_i$:

$$\boldsymbol{R}_v(\boldsymbol{\lambda}) = \left(\frac{\partial \boldsymbol{F}_{v,i-1/2}}{\partial \boldsymbol{q}_i}\frac{\partial \boldsymbol{q}_i}{\partial \boldsymbol{Q}_i}\right)^T (\boldsymbol{\lambda}_{i-1}-\boldsymbol{\lambda}_i)+\left(\frac{\partial \boldsymbol{F}_{v,i+1/2}}{\partial \boldsymbol{q}_i}\frac{\partial \boldsymbol{q}_i}{\partial \boldsymbol{Q}_i}\right)^T (\boldsymbol{\lambda}_i-\boldsymbol{\lambda}_{i+1}) \tag{7}$$

The viscous flux term of adjoint equation adopted the thin-layer approximation consistent with the flow equation. The flux Jacobian matrix in the above equation had been given in reference[2], which would not be repeated in this paper.

2.2 Viscosity Coefficient Variation

Under the condition of the thin-layer approximation, the variation of viscous term could be written as follows:

$$\begin{aligned}\delta \boldsymbol{F}_v &= \delta\left(\frac{M_\infty \mu}{Re_{\tilde{L}_R} J}\begin{pmatrix}0\\ \phi_1 u_\xi + n_{\xi,x}\phi_2\\ \phi_1 v_\xi + n_{\xi,y}\phi_2\\ \phi_1 w_\xi + n_{\xi,z}\phi_2\\ \phi_1 (p/\rho)_\xi \frac{1}{\mu}\left(\frac{\mu_l}{Pr_l}+\frac{\mu_T}{Pr_T}\right)\frac{\gamma}{\gamma-1}\\ +uf_{v2}+vf_{v3}+wf_{v4}\end{pmatrix}\right) \\ &= \delta\left(heat_{\mu_l}\right)+\delta\left(heat_{\mu_T}\right)+\delta\left(stress_\mu\right)+\delta\left(stress_{fix,\mu}\right)\end{aligned} \tag{8}$$

where:

$$\delta\left(heat_{\mu_l}\right) = \begin{pmatrix}0 & 0 & 0 & 0 & \phi_1 (p/\rho)_\xi \frac{1}{Pr_l}\frac{\gamma}{\gamma-1}\end{pmatrix}^T \delta\left(\frac{M_\infty \mu_l}{Re_{\tilde{L}_R} J}\right) = ① \times \frac{\partial \mu_l}{\partial \mathbf{Q}}\delta \mathbf{Q} \tag{9}$$

$$\delta\left(heat_{\mu_T}\right)=\begin{pmatrix}0 & 0 & 0 & 0 & \phi_1\left(p/\rho\right)_\xi\end{pmatrix}\frac{1}{Pr_T}\frac{\gamma}{\gamma-1}\Bigg)^T\delta\left(\frac{M_\infty\mu_T}{Re_{\tilde{L}_R}J}\right)=②\times\frac{\partial\mu_T}{\partial\mathbf{Q}}\delta\mathbf{Q} \tag{10}$$

$$\delta\left(stress_\mu\right)=\begin{pmatrix}0\\ \phi_1u_\xi+n_{\xi,x}\phi_2\\ \phi_1v_\xi+n_{\xi,y}\phi_2\\ \phi_1w_\xi+n_{\xi,z}\phi_2\\ uf_{v2}+vf_{v3}+wf_{v4}\end{pmatrix}\delta\left(\frac{M_\infty\mu}{Re_{\tilde{L}_R}J}\right)=③\times\left(\frac{\partial\mu_l}{\partial\mathbf{Q}}\delta\mathbf{Q}+\frac{\partial\mu_T}{\partial\mathbf{Q}}\delta\mathbf{Q}\right) \tag{11}$$

$$\delta\left(stress_{fix,\mu}\right)=\frac{M_\infty\mu}{Re_{\tilde{L}_R}J}\delta\begin{pmatrix}0\\ \phi_1u_\xi+n_{\xi,x}\phi_2\\ \phi_1v_\xi+n_{\xi,y}\phi_2\\ \phi_1w_\xi+n_{\xi,z}\phi_2\\ \phi_1\left(p/\rho\right)_\xi\left(\frac{1}{\mu}\left(\frac{\mu_l}{Pr_l}+\frac{\mu_T}{Pr_T}\right)\frac{\gamma}{\gamma-1}\right)_{fix}\\ +uf_{v2}+vf_{v3}+wf_{v4}\end{pmatrix} \tag{12}$$

The assumption of constant viscosity actually ignored the first to third terms of the Eq. (8). In the calculation of flow field, the calculation of laminar viscosity coefficient was different from that of turbulence viscosity coefficient. The laminar viscosity coefficient was directly calculated by using the total temperature of the cell-interface, while the turbulence viscosity coefficient was obtained by averaging the cell center values; In addition, the number of stencils involved in SA and SST model was different. When only considering the variation of laminar viscosity coefficient:

$$\boldsymbol{R}_{v,\mu_l}(\boldsymbol{\lambda})=\left(\frac{\partial\boldsymbol{F}_{v,\mu_l,i-1/2}}{\partial\boldsymbol{q}_i}\frac{\partial\boldsymbol{q}_i}{\partial\boldsymbol{Q}_i}\right)^T\left(\boldsymbol{\lambda}_{i-1}-\boldsymbol{\lambda}_i\right)+\left(\frac{\partial\boldsymbol{F}_{v,\mu_l,i+1/2}}{\partial\boldsymbol{q}_i}\frac{\partial\boldsymbol{q}_i}{\partial\boldsymbol{Q}_i}\right)^T\left(\boldsymbol{\lambda}_i-\boldsymbol{\lambda}_{i+1}\right) \tag{13}$$

where:

$$\frac{\partial\boldsymbol{F}_{v,\mu_l,i+1/2}}{\partial\boldsymbol{q}_i}=\left(①_{i+1/2}+③_{i+1/2}\right)\times\frac{\partial\mu_{l,i+1/2}}{\partial\boldsymbol{q}_i} \tag{14}$$

according to the form of the cell-interface laminar viscosity:

$$\begin{aligned}\frac{\partial\mu_{l,i+1/2}}{\partial\boldsymbol{q}_i}&=\frac{\partial\mu_{l,i+1/2}}{\partial T_{i+1/2}}\frac{\partial T_{i+1/2}}{\partial\boldsymbol{q}_i}=\frac{\partial}{\partial\boldsymbol{q}_i}\left(T^{\frac{3}{2}}\frac{1+C'}{T+C'}\right)\\&=\left(\frac{3}{2}T_{i+1/2}+\frac{-1}{T_{i+1/2}+C'}\right)\mu_{l,i+1/2}\begin{pmatrix}-1/\rho_i & 0 & 0 & 0 & 1/p_i\end{pmatrix}\frac{1}{T_i}\end{aligned} \tag{15}$$

The boundary condition matrix treatment was consistent with the inviscid term, and the flux stencil of the boundary was shown in Fig. 1. In this paper, the starting and ending boundary of the grid were referred as ST_IN1 (2), ST_IN2 (3), ED_IN1 (jmax), ED_IN2 (jmax - 1).

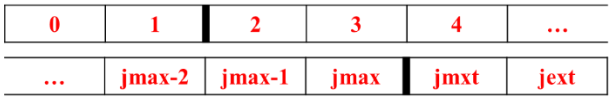

Fig. 1 Flux stencil of the boundary

Spalart-Allmaras Turbulence Model

The left term of the adjoint equation obtained from the variation of viscosity coefficient in the Spalart-Allmaras turbulence model was as follows:

$$\boldsymbol{R}_{v,\mu_T}(\boldsymbol{\lambda})=\left(\frac{\partial \boldsymbol{F}_{v,\mu_T,i-1/2}}{\partial \boldsymbol{q}_i}\frac{\partial \boldsymbol{q}_i}{\partial \boldsymbol{Q}_i}\right)^T\left(\boldsymbol{\lambda}_{i-1}-\boldsymbol{\lambda}_i\right)+\left(\frac{\partial \boldsymbol{F}_{v,\mu_T,i+1/2}}{\partial \boldsymbol{q}_i}\frac{\partial \boldsymbol{q}_i}{\partial \boldsymbol{Q}_i}\right)^T\left(\boldsymbol{\lambda}_i-\boldsymbol{\lambda}_{i+1}\right) \tag{16}$$

where:

$$\frac{\partial \boldsymbol{F}_{v,\mu_T,i+1/2}}{\partial \boldsymbol{q}_i}=\left(②_{i+1/2}+③_{i+1/2}\right)\times\frac{\partial \mu_{T,i+1/2}}{\partial \boldsymbol{q}_i} \tag{17}$$

according to the form of the cell-interface turbulence viscosity:

$$\frac{\partial \mu_{T,i+1/2}}{\partial \boldsymbol{q}_i}=\frac{\partial \mu_{T,i+1/2}}{\partial \mu_{T,i}}\frac{\partial \mu_{T,i}}{\partial \boldsymbol{q}_i}=\frac{1}{2}\left(\mu_{T,i}\left(1/\rho_i \quad 0 \quad 0 \quad 0 \quad 0\right)+\rho_i\hat{v}_i\frac{\partial f_{v1,i}}{\partial \boldsymbol{q}_i}\right) \tag{18}$$

where:

$$\frac{\partial f_{v1,i}}{\partial \boldsymbol{q}_i}=\frac{\partial}{\partial q}\left(\frac{\chi_i^3}{\chi_i^3+C_{v1}^3}\right)=\frac{3\chi_i^2C_{v1}^3}{\left(\chi_i^3+C_{v1}^3\right)^2}\frac{\partial \chi_i}{\partial \boldsymbol{q}_i} \tag{19}$$

$$\frac{\partial \chi_i}{\partial \boldsymbol{q}_i}=-\frac{\chi_i}{\mu_{l,i}}\left(\frac{\partial \mu_{l,i}}{\partial \boldsymbol{q}_i}+\mu_{l,i}\left(-1/\rho_i \quad 0 \quad 0 \quad 0 \quad 0\right)\right),\mu_{l,i}=\rho\hat{v}_i \tag{20}$$

Special attention should be paid to the wall boundary condition of the turbulence model, with ST_IN1 boundary as an example:

$$\begin{aligned}\boldsymbol{R}_{v,\mu_T}(\boldsymbol{\lambda})=&\left(\frac{\partial \boldsymbol{F}_{v,\mu_T,i-1/2}}{\partial \boldsymbol{q}_{i-1}}\frac{\partial \boldsymbol{q}_{i-1}}{\partial \boldsymbol{Q}_i}+\frac{\partial \boldsymbol{F}_{v,\mu_T,i-1/2}}{\partial \boldsymbol{q}_i}\frac{\partial \boldsymbol{q}_i}{\partial \boldsymbol{Q}_i}\right)^T\left(-\boldsymbol{\lambda}_i\right)\\&+\left(\frac{\partial \boldsymbol{F}_{v,\mu_T,i+1/2}}{\partial \boldsymbol{q}_i}\frac{\partial \boldsymbol{q}_i}{\partial \boldsymbol{Q}_i}\right)^T\left(\boldsymbol{\lambda}_i-\boldsymbol{\lambda}_{i+1}\right)\end{aligned} \tag{21}$$

Due to the forced setting of the turbulence viscosity coefficient to 0, it was directly treated as $\partial \boldsymbol{F}_{v,\mu_T,i-1/2} \big/ \partial \boldsymbol{Q}_i = 0$.

Menter's k-ω SST Turbulence Model

Due to the direct use of vorticity $\Omega_i = \Omega_i\left(\boldsymbol{Q}_{i-1}, \boldsymbol{Q}_i, \boldsymbol{Q}_{i+1}\right)$ in the calculation of viscosity coefficient in the SST turbulence model, there were more stencils compared to the SA turbulence model. Therefore, the left term of the adjoint equation of the turbulence model variation was:

$$\begin{aligned}\boldsymbol{R}_{v,\mu_T}(\boldsymbol{\lambda}) = &\left(\frac{\partial \boldsymbol{F}_{v,\mu_T,i-3/2}}{\partial \boldsymbol{q}_i}\frac{\partial \boldsymbol{q}_i}{\partial \boldsymbol{Q}_i}\right)^T\left(\boldsymbol{\lambda}_{i-2}-\boldsymbol{\lambda}_{i-1}\right)+\left(\frac{\partial \boldsymbol{F}_{v,\mu_T,i-1/2}}{\partial \boldsymbol{q}_i}\frac{\partial \boldsymbol{q}_i}{\partial \boldsymbol{Q}_i}\right)^T\left(\boldsymbol{\lambda}_{i-1}-\boldsymbol{\lambda}_{i}\right)+\\ &\left(\frac{\partial \boldsymbol{F}_{v,\mu_T,i+1/2}}{\partial \boldsymbol{q}_i}\frac{\partial \boldsymbol{q}_i}{\partial \boldsymbol{Q}_i}\right)^T\left(\boldsymbol{\lambda}_{i}-\boldsymbol{\lambda}_{i+1}\right)+\left(\frac{\partial \boldsymbol{F}_{v,\mu_T,i+3/2}}{\partial \boldsymbol{q}_i}\frac{\partial \boldsymbol{q}_i}{\partial \boldsymbol{Q}_i}\right)^T\left(\boldsymbol{\lambda}_{i+1}-\boldsymbol{\lambda}_{i+2}\right)\end{aligned} \tag{22}$$

where:

$$\frac{\partial \boldsymbol{F}_{v,\mu_T,i+1/2}}{\partial \boldsymbol{q}_i} = \left(②_{i+1/2}+③_{i+1/2}\right)\times\frac{\partial \mu_{T,i+1/2}}{\partial \boldsymbol{q}_i} \tag{23}$$

according to the form of the cell-interface turbulence viscosity:

$$\begin{aligned}\frac{\partial \mu_{T,i-3/2}}{\partial \boldsymbol{q}_i} &= \frac{\partial \mu_{T,i-3/2}}{\partial \mu_{T,i-1}}\frac{\partial \mu_{T,i-1}}{\partial \boldsymbol{q}_i}\\ \frac{\partial \mu_{T,i-1/2}}{\partial \boldsymbol{q}_i} &= \frac{\partial \mu_{T,i-1/2}}{\partial \mu_{T,i-1}}\frac{\partial \mu_{T,i-1}}{\partial \boldsymbol{q}_i}+\frac{\partial \mu_{T,i-1/2}}{\partial \mu_{T,i}}\frac{\partial \mu_{T,i}}{\partial \boldsymbol{q}_i}\\ \frac{\partial \mu_{T,i+1/2}}{\partial \boldsymbol{q}_i} &= \frac{\partial \mu_{T,i+1/2}}{\partial \mu_{T,i}}\frac{\partial \mu_{T,i}}{\partial \boldsymbol{q}_i}+\frac{\partial \mu_{T,i+1/2}}{\partial \mu_{T,i+1}}\frac{\partial \mu_{T,i+1}}{\partial \boldsymbol{q}_i}\\ \frac{\partial \mu_{T,i+3/2}}{\partial \boldsymbol{q}_i} &= \frac{\partial \mu_{T,i+3/2}}{\partial \mu_{T,i+1}}\frac{\partial \mu_{T,i+1}}{\partial \boldsymbol{q}_i}\end{aligned} \tag{24}$$

Based on the above analysis, the variation of turbulence viscosity coefficient needed to treat the follow parts:

$$\frac{\partial \mu_{T,i}}{\partial \boldsymbol{q}_{i-1}} \quad \frac{\partial \mu_{T,i}}{\partial \boldsymbol{q}_i} \quad \frac{\partial \mu_{T,i}}{\partial \boldsymbol{q}_{i+1}} \tag{25}$$

Due to the piecewise functions in the calculation of turbulence model, it was necessary to take derivatives for all parts and select the corresponding parts which was based on the calculation results of the turbulence model for iteration. In the flow field calculation, the ghost grid information exchanged directly by communicating the viscosity coefficient of the cells in other blocks, rather than the selection of the

piecewise function of the cells in other blocks. Therefore, in the adjoint equation calculation, it was necessary to pre-calculate a step before the iteration to communicate the selection of the cells in other blocks. Due to the complexity of the treatment, this article only took the selection of the minimum value as an example, and the selection of the minimum value was represented by *kw - sst - min - selection* , where:

$$kw\text{-}sst\text{-}min\text{-}selection=\begin{cases}1,\mu_T=\dfrac{\rho k}{\omega}\\ 2,\mu_T=\dfrac{a_1\rho k}{\Omega F_2}\left(\dfrac{Re}{M_\infty}\right)\end{cases} \tag{26}$$

when $kw\text{-}sst\text{-}min\text{-}selection=1$:

$$\begin{aligned}&\frac{\partial\mu_{T,i}}{\partial\boldsymbol{q}_{i-1}}=0\\ &\frac{\partial\mu_{T,i}}{\partial\boldsymbol{q}_i}=\mu_{T,i}\begin{pmatrix}-1/\rho_i & 0 & 0 & 0 & 0\end{pmatrix}\\ &\frac{\partial\mu_{T,i}}{\partial\boldsymbol{q}_{i+1}}=0\end{aligned} \tag{27}$$

when $kw\text{-}sst\text{-}min\text{-}selection=2$:

$$\begin{aligned}&\frac{\partial\mu_{T,i}}{\partial\boldsymbol{q}_{i-1}}=\mu_{T,i}\frac{-1}{\Omega_i}\frac{\partial\Omega_i}{\partial\boldsymbol{q}_{i-1}}\\ &\frac{\partial\mu_{T,i}}{\partial\boldsymbol{q}_i}=\mu_{T,i}\begin{pmatrix}-1/\rho_i & 0 & 0 & 0 & 0\end{pmatrix}+\mu_{T,i}\frac{-1}{\Omega_i}\frac{\partial\Omega_i}{\partial\boldsymbol{q}_i}+\mu_{T,i}\frac{-1}{F_{2,i}}\frac{\partial F_{2,i}}{\partial\boldsymbol{q}_i}\\ &\frac{\partial\mu_{T,i}}{\partial\boldsymbol{q}_{i+1}}=\mu_{T,i}\frac{-1}{\Omega_i}\frac{\partial\Omega_i}{\partial\boldsymbol{q}_{i+1}}\end{aligned} \tag{28}$$

where $\Omega=\sqrt{\omega_1^2+\omega_2^2+\omega_3^2}\Big/J=\left\|\boldsymbol{rot}\left(u,v,w\right)\right\|\Big/J$, further derivation would not be repeated.

In the treatment of boundary conditions, the SST model was similar to the inviscid term that based on the Van Leer scheme. However, due to the fact that the cell center vorticity was only related to three cells, and in a direction such as the ξ direction, the forward and backward flux of the inviscid term of a single cell were related to a total of five cells. Therefore, the boundary treatment of the SST model was actually simpler than that of the inviscid term based on the Van Leer scheme, and only ST_IN1 needed to be treat.

3 Research on the Variational Effect of Viscosity Coefficient

3.1 The Influence on Adjoint Equation and Gradient Accuracy:

In this section the influence of viscosity coefficient variation on the adjoint equation calculation and gradient accuracy was studied. The FFD approach[16] based on NURBS basis function was used for wing parameterization. The shape and FFD lattice of ONERA M6 were shown in Fig. 2. There were 70 design variables in total, 5 sections were arranged along the span, and 7 design variables were arranged on the upper and lower surfaces of each section in the streamwise. The design variables used in gradient validate were the root section design variables.

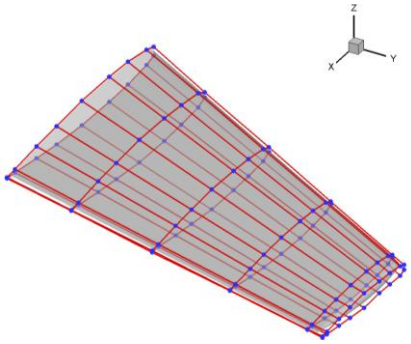

Fig. 2 FFD Lattice and Design Variables

The calculation condition was Ma=0.84, Re=6.8×10^6, C_L=0.2452. Due to the fact that the calculation of laminar viscosity coefficient was independent of the turbulence model and the variation of laminar viscosity coefficient was simple, the influence of only considering the variation of laminar viscosity coefficient was not carried out. The influence of the variation of turbulence model shown in Fig. 3 and Fig. 4 actually included the variation of laminar viscosity coefficient, and the variation of turbulence model in the following text all include the variation term of laminar viscosity coefficient.

The convergence of the adjoint equation showed that the variation of viscosity coefficient had a small influence on the robustness of the adjoint equation. This was different from the conclusion of reference[15]. The gradient comparisons showed that the variation of viscosity coefficient had a certain influence on the gradient accuracy. Due to the large influence of disturbance step on finite difference, it was not used as a reference here. The influence of the viscosity coefficient variation to the gradient corresponding to the two turbulence models was relatively consistent when compared to the fixed viscosity coefficient. Variables 8 to 14 were on the upper surface, where there were supersonic flow and shock boundary layer interference separation, and the flow viscosity had a great influence on the it; Variables 1 to 7 were on the lower sur-

face, where the flow were relaxation and influence of viscosity coefficient variation was small, which was consistent with the flow.

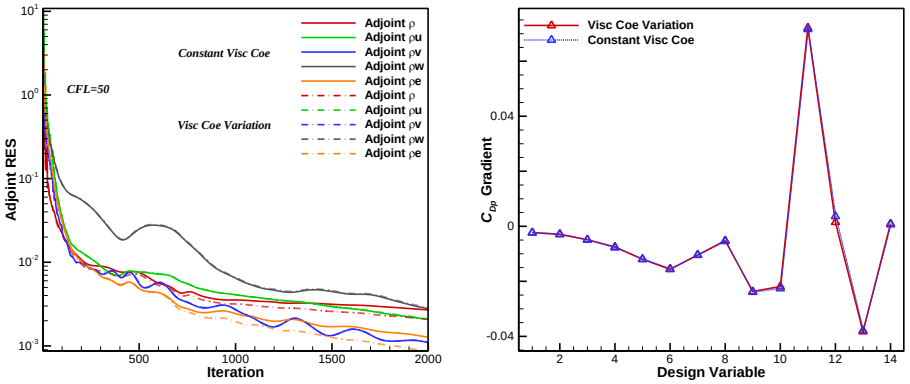

Fig. 3 Influence of SA turbulence model variation on the convergence of adjoint equations and gradient accuracy

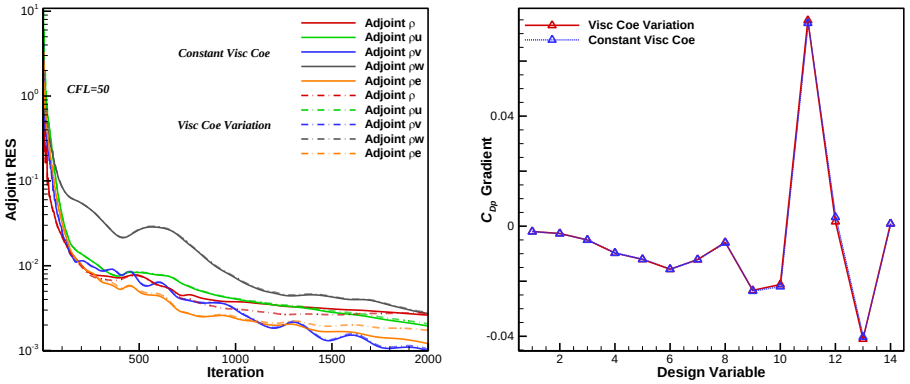

Fig. 4 Influence of SST turbulence model variation on the convergence of adjoint equations and gradient accuracy

3.2 Influence on the aerodynamic optimization design

In this section a study on the influence of viscosity coefficient variation on optimization design was conducted. The initial states were the cruise state optimization results of the CRM wing body under the assumption of constant viscosity. The optimization design model was shown in the equation:

$$\begin{aligned} \min: \quad & F = C_{Dp}(\boldsymbol{x}) \\ s.t.: \quad & C_L(\boldsymbol{x}) = 0.5 \\ & t_{m,n}(\boldsymbol{x}) \geq t_{m,n}(\boldsymbol{x}_0) \quad m,n = 1,2,...,9 \end{aligned} \tag{29}$$

The initial value of the viscosity coefficient variation optimization design for SST turbulence model was x_{62}, and x_{23} for SA turbulence model.

(1) Menter's k-ω SST Turbulence Model

The convergence of the viscosity coefficient variation optimization design of the SST turbulence model was shown in Fig. 5, and the optimization design met the convergence requirements at step 86. The pressure drag of step 62 was 148.8 counts and 148.1 counts when stop, with a decrease of 0.7 count, indicating that there was still some optimization space for the optimization problem of the cruise state under the use of the viscosity coefficient variation method in this article, which could further improve the cruise performance.

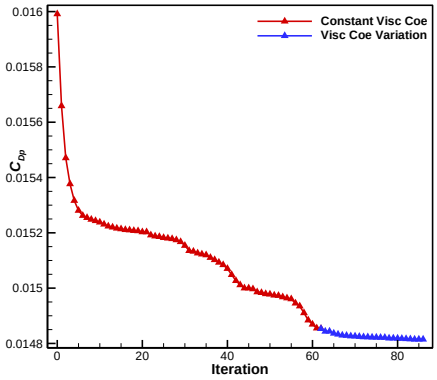

Fig. 5 Optimize convergence history

The comparison of pressure distribution was shown in Fig. 6, and the sectional pressure coefficient distribution was shown in Fig. 7. The black color represented the constant viscosity optimization result, while the red color represented the viscosity variation optimization result. The pressure distribution was smoother when considering the viscosity coefficient variation, which further reducing the pressure drag.

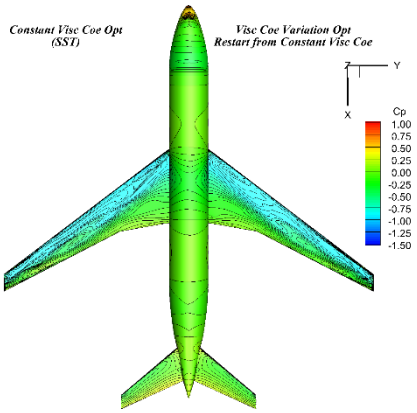

Fig. 6 Pressure distribution of x_{62} (left) and x_{86} (right)

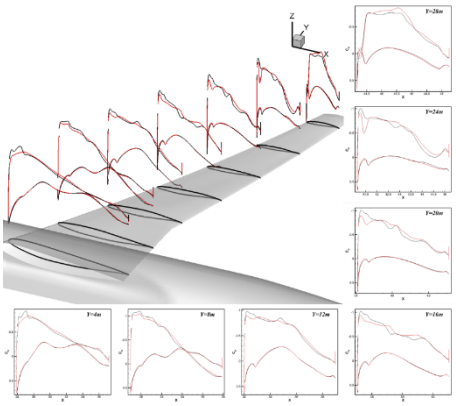

Fig. 7 Sectional pressure coefficient distribution of x_{62}(black) and x_{86}(red)

(2) Spalart Allmaras Turbulence Model

The convergence of the viscosity coefficient variation optimization design of the SA turbulence model was shown in Fig. 8, and the optimization design met the convergence requirements at step 41. The pressure drag of step 23 was 155.5 counts and 154.3 counts when stop, with a decrease of 1.2 count, verifying the design potential of the viscosity coefficient variation method.

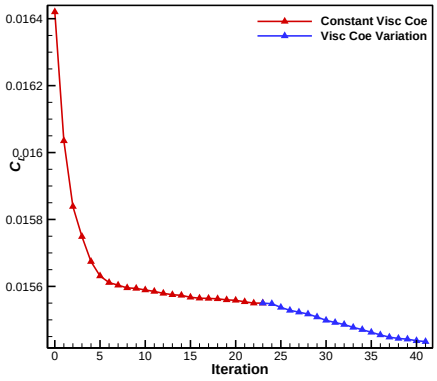

Fig. 8 Optimize convergence history

The comparison of pressure distribution was shown in Fig. 9, and the sectional pressure coefficient distribution was shown in Fig. 10. The weak shock wave intensity at kink position of the wing was smaller when considering viscosity coefficient variation, and the pressure difference drag was lower.

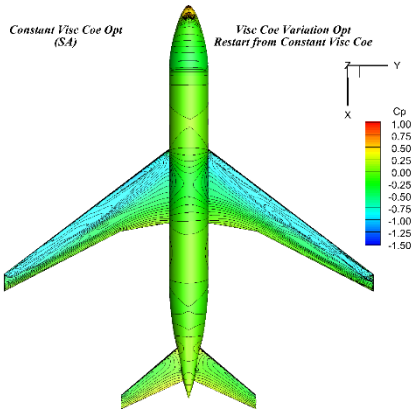

Fig. 9 Pressure distribution of x_{23} (left) and x_{41} (right)

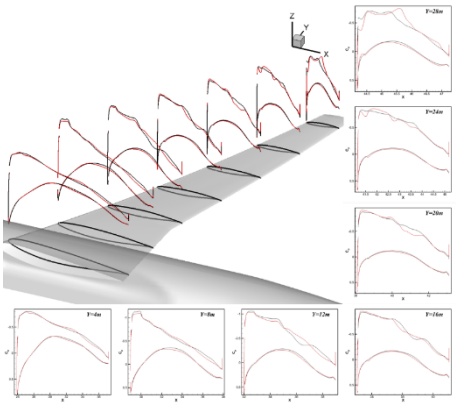

Fig. 10 Sectional pressure coefficient distribution of x_{23}(black) and x_{41}(red)

4 Conclusion

In this article the aerodynamic adjoint method with the variation of viscosity coefficient was established based on Spalart-Allmaras and Menter's k-ω SST turbulence model. The aerodynamic adjoint method with the variation of viscosity coefficient was analyzed by using M6 wing case to demonstrate its robustness and influence on gradient; The optimization performance of this method was tested by the CRM wing-body optimization cases, and the conclusions were as follows:

(1) The viscosity coefficient variation had little influence on the robustness of adjoint equation and the accuracy of gradient.

(2) The aerodynamic adjoint method with the variation of viscosity coefficient established in this article could further improve the performance of aircraft optimization design. The variation of viscosity coefficient in both turbulence models could improve aircraft cruise performance.

(3) The aerodynamic adjoint method that considering the variation of viscosity coefficient laid the foundation for the optimization design of laminar flow, which was also the research to be carried out in the future.

References

1. Jiangtao H. Sensitivity Analysis of Design Variables Considering Intake and Exhaust Effects. Journal of Propulsion Technology 2019(002):040. (In Chinese)
2. Jiangtao H. Investigation of gradient computation based on discrete adjoint method. Acta Aerodynamica Sinica 2017; 35(4):554-62. (In Chinese)

3. Jiangtao H. Numerical study of aero-structural multidisciplinary lagged coupled adjoint system for aircraft. Acta Aeronautica et Astronautica Sinica 2018; 39(005):96-107. (In Chinese)
4. Jiangtao H, Jing Y. Multi-disciplinary Optimization of Large Civil Aircraft Using a Coupled Aero-Structural Adjoint Approach. The Proceedings of the 2018 Asia-Pacific International Symposium on Aerospace Technology (APISAT 2018). 2019; 1042-54.
5. Rallabhandi S. Sonic Boom Adjoint Methodology and its Applications. 29th AIAA Applied Aerodynamics Conference. 2011.
6. Lin Z. Three-Dimensional Aerodynamic/Stealth Optimization Based on Adjoint Sensitivity Analysis for Scattering Problem. AIAA Journal 2020:1-14.
7. Lin Z. Three Dimensional Radar Cross Section Geometr ic Sensitivity Calculation Based on Discrete Adjoint Equation. Acta Aeronautica et Astronautica Sinica 2020. (In Chinese)
8. Nielsen. Recent Improvements in Aerodynamics Design Optimization on Unstructured Meshes. AIAA Journal 2002.
9. Dwight R, Brezillon J. Effect of Various Approximations of the Discrete Adjoint on Gradient-Based Optimization. Proceedings of the 44th AIAA Aerospace Sciences Meeting and Exhibit, Reno NV AIAA-2006-0690. 2006.
10. Carrier G. Gradient-Based Aerodynamic Optimization with the elsA Software. 52nd Aerospace Sciences Meeting - AIAA SciTech 2014. 2014.
11. Mader CA. ADflow: An Open-Source Computational Fluid Dynamics Solver for Aerodynamic and Multidisciplinary Optimization. Journal of Aerospace Information Systems 2020; 17(9):508-27.
12. Yingtao Z. Aerodynamic design method based on N-S equations and discrete adjoint approach. Acta Aerodynamica Sinica 2010; 27(1):67-72. (In Chinese)
13. Bing L. Discrete Adjoint Optimization Method for 3D Unstructured Grid. Acta Aeronautica Et Astronautica Sinica 2014; 35(3):674-86.
14. Jun D. Optimization Design Method of Aircraft Boundary Characteristics Based on Upwind Scheme Adjoint Equation. Journal of Beijing University of Aeronautics and Astronautics:1-20. (In Chinese)
15. Hangkong W. Influence of “frozen viscosity assumption” on solution and gradient accuracy of adjoint system. Acta Aeronautica et Astronautica Sinica 2022; 43(07):212-28. (In Chinese)
16. Kenway G, Kennedy GJ. A CAD-Free Approach to High-Fidelity Aerostructural Optimization. Aiaa/issmo Multidisciplinary Analysis Optimization Conference. 2010.